

Generation of Attosecond X-ray and gamma-ray via Compton backscattering

Sang-Young Chung, Moohyun Yoon and Dong Eon Kim*

Physics Department, POSTECH,
San 31 Hyojadong, Nam Ku, Pohang, Kyungbuk, 790-784, KOREA
kimd@postech.ac.kr

Abstract: The generation of an isolated attosecond gamma-ray pulse utilizing Compton backscattering of a relativistic electron bunch has been investigated. The energy of the electron bunch is modulated while the electron bunch interacts with a co-propagating few-cycle CEP (carrier envelope phase)-locked laser in a single-period wiggler. The energy-modulated electron bunch interacts with a counter-propagating driver laser, producing Compton back-scattered radiation. The energy modulation of the electron bunch is duplicated to the temporal modulation of the photon energy of Compton back-scattered radiation. The spectral filtering using a crystal spectrometer allows one to obtain an isolated attosecond gamma-ray.

© 2009 Optical Society of America

OCIS codes: (320.5550) Pulses; (260.7120) Ultrafast phenomena; (290.1350) Backscattering

References and links

1. G. Sansone, E. Benedetti, F. Calegari, C. Vozzi, L. Avaldi, R. Flammini, L. Poletto, P. Villoresi, C. Altucci, R. Velotta, S. Stagira, S. De Silvestri, and M. Nisoli, "Isolated single-cycle attosecond pulses," *Science* **314**(5798), 443–446 (2006).
2. R. Kienberger, E. Goulielmakis, M. Uiberacker, A. Baltuska, V. Yakovlev, F. Bammer, A. Scrinzi, Th. Westerwalbesloh, U. Kleineberg, U. Heinzmann, M. Drescher, and F. Krausz, "Atomic transient recorder," *Nature* **427**(6977), 817–821 (2004).
3. M. Uiberacker, T. Uphues, M. Schultze, A. J. Verhoef, V. Yakovlev, M. F. Kling, J. Rauschenberger, N. M. Kabachnik, H. Schröder, M. Lezius, K. L. Kompa, H. G. Muller, M. J. Vrakking, S. Hendel, U. Kleineberg, U. Heinzmann, M. Drescher, and F. Krausz, "Attosecond real-time observation of electron tunnelling in atoms," *Nature* **446**(7136), 627–632 (2007).
4. E. Goulielmakis, M. Uiberacker, R. Kienberger, A. Baltuska, V. Yakovlev, A. Scrinzi, Th. Westerwalbesloh, U. Kleineberg, U. Heinzmann, M. Drescher, and F. Krausz, "Direct measurement of light waves," *Science* **305**(5688), 1267–1269 (2004).
5. M. Drescher, M. Hentschel, R. Kienberger, M. Uiberacker, V. Yakovlev, A. Scrinzi, Th. Westerwalbesloh, U. Kleineberg, U. Heinzmann, and F. Krausz, "Time-resolved atomic inner-shell spectroscopy," *Nature* **419**(6909), 803–807 (2002).
6. G. Farkas and C. Toth, "Proposal for attosecond light pulse generation using laser induced multiple-harmonic conversion processes in rare gases," *Phys. Lett. A* **168**(5-6), 447–450 (1992).
7. A. A. Zholents and W. M. Fawley, "Proposal for intense attosecond radiation from an x-ray free-electron laser," *Phys. Rev. Lett.* **92**(22), 224801 (2004).
8. A. A. Zholents and G. Penn, "Obtaining attosecond x-ray pulses using a self-amplified spontaneous emission free electron laser," *Phys. Rev. ST Accel. Beams* **8**(5), 050704 (2005).
9. P. Emma, K. Bane, M. Cornacchia, Z. Huang, H. Schlarb, G. Stupakov, and D. Walz, "Femtosecond and subfemtosecond x-ray pulses from a self-amplified spontaneous-emission-based free-electron laser," *Phys. Rev. Lett.* **92**(7), 074801 (2004).
10. E. L. Saldin, E. A. Schneidmiller, and M. V. Yurkov, "A new technique to generate 100 GW-level attosecond X-ray pulses from the X-ray SASE FELs," *Opt. Commun.* **239**(1-3), 161–172 (2004).
11. P. Lan, P. Lu, W. Cao, and X. Wang, "Attosecond and zeptosecond x-ray pulses via nonlinear Thomson backscattering," *Phys. Rev. E Stat. Nonlin. Soft Matter Phys.* **72**(6 Pt 2), 066501 (2005).

12. A. E. Kaplan and P. L. Shkolnikov, "Lasetron: a proposed source of powerful nuclear-time-scale electromagnetic bursts," *Phys. Rev. Lett.* **88**(7), 074801 (2002).
13. F. V. Hartemann, W. J. Brown, D. J. Gibson, S. G. Anderson, A. M. Tremaine, P. T. Springer, A. J. Wootton, E. P. Hartouni, and C. P. J. Barty, "High-energy scaling of Compton scattering light sources," *Phys. Rev. ST Accel. Beams* **8**(10), 100702 (2005).
14. M. S. Dewey, E. G. Kessler, G. L. Greene, R. D. Deslattes, H. Borner, and J. Jolie, "Fundamental physics using ultrahigh resolution gamma spectroscopy," *Nucl. Instrum. Methods Phys. Res. A* **284**(1), 151–155 (1989).
15. G. L. Borchert, W. Scheck, and O. W. B. Schult, "Curved crystal spectrometer for precise energy measurements of gamma rays from 30 to 1500 keV," *Nucl. Instrum. Methods* **124**(1), 107–117 (1975).
16. G. L. Borchert, J. Bojowald, A. Ercan, H. Labus, Th. Rose, and O. W. B. Schult, "Curved crystal spectrometer for high-resolution in-beam spectroscopy of x-rays and low-energy gamma rays," *Nucl. Instrum. Methods Phys. Res. A* **245**(2-3), 393–401 (1986).
17. E. G. Kessler, M. S. Dewey, R. D. Deslattes, A. Henins, H. G. Börner, M. Jentsche, and H. Lehmann, "The GAMS4 flat crystal facility," *Nucl. Instrum. Methods Phys. Res. A* **457**(1-2), 187–202 (2001).
18. A. Yariv, *Optical Electronics 4th ed.* (Holt, Rinehart and Winston Inc., Philadelphia, 1991) pp. 47–48.
19. K. Lee, Y. H. Cha, M. S. Shin, B. H. Kim, and D. Kim, "Temporal and spatial characterization of harmonics structures of relativistic nonlinear Thomson scattering," *Opt. Express* **11**, 309–316 (2003).
20. K. Lee, Y. H. Cha, M. S. Shin, B. H. Kim, and D. Kim, "Relativistic nonlinear Thomson scattering as attosecond x-ray source," *Phys. Rev. E Stat. Nonlin. Soft Matter Phys.* **67**(2 Pt 2), 026502 (2003).
21. K. Lee, B. H. Kim, and D. Kim, "Coherent radiation of relativistic nonlinear Thomson scattering," *Phys. Plasmas* **12**(4), 043107 (2005).
22. W. J. Brown and F. V. Hartemann, "Three-dimensional time and frequency-domain theory of femtosecond x-ray pulse generation through Thomson scattering," *Phys. Rev. ST Accel. Beams* **7**(6), 060703 (2004).
23. K. J. Weeks, V. N. Litvinenko, and J. M. J. Madey, "The Compton backscattering process and radiotherapy," *Med. Phys.* **24**(3), 417–423 (1997).
24. C. A. Brau, *Free-Electron Lasers* (Academic Press Inc., New York, 1990) pp. 64–85.
25. A 5 ns, 1064 nm pulsed laser of 1 J at 5 kHz is under development at Institute of Laser Engineering, Osaka University, Japan, presented in Workshop on Advanced Technology of lasers for understanding of plasma physics, KAIST, Daejeon, Republic of Korea, Feb. 13–14, 2009.
26. A. L. Cavalieri, D. M. Fritz, S. H. Lee, P. H. Bucksbaum, D. A. Reis, J. Rudati, D. M. Mills, P. H. Fuoss, G. B. Stephenson, C. C. Kao, D. P. Siddons, D. P. Lowney, A. G. Macphie, D. Weinstein, R. W. Falcone, R. Pahl, J. Als-Nielsen, C. Blome, S. Düsterer, R. Ischebeck, H. Schlarb, H. Schulte-Schrepping, Th. Tschentscher, J. Schneider, O. Hignette, F. Sette, K. Sokolowski-Tinten, H. N. Chapman, R. W. Lee, T. N. Hansen, O. Synnørgren, J. Larsson, S. Techert, J. Sheppard, J. S. Wark, M. Bergh, C. Caleman, G. Huldt, D. van der Spoel, N. Timneanu, J. Hajdu, R. A. Akre, E. Bong, P. Emma, P. Krejčík, J. Arthur, S. Brennan, K. J. Gaffney, A. M. Lindenberg, K. Luening, and J. B. Hastings, "Clocking femtosecond X rays," *Phys. Rev. Lett.* **94**(11), 114801 (2005).

1. Introduction

Femto-science has increased our understanding of ultrafast dynamics in physics and chemistry over the past decade. The recent success in the generation [1, 2] of an isolated attosecond pulse and its applications [3, 4, 5] has opened a door to the investigation of even faster processes in nature such as electronic transitions in atoms and molecules. Also, in the nuclear physics an isolated ultrashort gamma-ray pulse will allow to trace *ultrafast* nuclear dynamics. There is a growing demand for the generation of an isolated attosecond pulse at different photon energies with a higher photon flux.

In the XUV and the hard x-ray region, experiments for attosecond pulse generation were carried out or proposed. An isolated attosecond XUV pulse was successfully produced using the high-harmonics generation (HHG) method from a neutral gas [1, 6]. In the photon energy of 10 keV or lower, several ideas have been put forward for attosecond pulse generation [7, 8, 9, 10]. Simulation studies have been for the zeptosecond gamma-ray pulse generation by the nonlinear Thomson scattering between a tightly focused laser and a counter-propagating electron [11] or by a laser based synchrotron [12]. However, these studies have not been done for a realistic electron bunch but for a single electron. The ideas are not tangible. To the authors' knowledge, there is no applicable proposal to generate isolated attosecond gamma-ray pulses using an electron bunch.

In this paper, we propose a method to generate attosecond gamma-ray pulses utilizing the

combination of Compton backscattering and energy modulation of a relativistic electron bunch. The Compton backscattering, a head-on collision between a laser and an electron bunch, is known as a good method to generate gamma-ray pulse because not only the photon energy is tunable by changing the laser photon energy or the electron energy but also the radiation is polarized [13]. The energy modulation of an electron bunch by a co-propagating laser was used for the generation of an attosecond x-ray pulse with an electron beam and undulator [7, 8]. The energy modulation scheme is here further optimized for the attosecond gamma-ray generation. The radiated photon energy is tunable and reaches several ten keV to MeVs.

2. Scheme

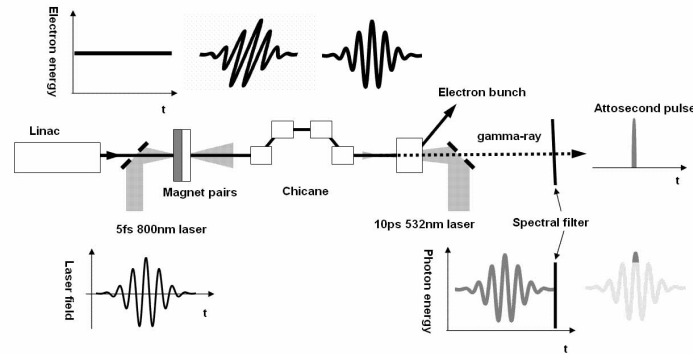


Fig. 1. Schematic diagram of the setup for the energy modulation of electron bunch, Compton backscattering and attosecond gamma-ray pulse generation. The upper thick black lines show the energy distributions of the electron bunch at the each step. The lower black thin line is graph about the laser field and gray thick line for the photon energy distribution of the radiation.

Figure 1 shows the schematic diagram. A few-cycle pulsed laser propagates in the $+z$ -direction and an electron bunch co-propagates with the laser. The laser is carrier envelope phase (CEP)-locked and polarized in the x -direction. Both of the laser and the electron bunch goes through a single-period wiggler. The wiggler provides magnetic fields in the $+y$ and $-y$ direction. Both the laser and the electron bunch are focused on the z -axis at the center of the wiggler and are adjusted in space and time to overlap each other near focus. The interaction of the electron bunch with the co-propagating laser results in the energy modulation of the electron beam. The shape of the energy modulation is the same as the laser field as shown in Fig. 1 and 2. The accelerated electrons go faster and the decelerated electrons move slowly so that the temporal profile of the electron energy is slanted [Fig. 1]. The chicane is then needed to compensate the difference in the arrival times and correct the slant in the energy modulation. After the chicane, the energy-modulated electron bunch interacts with another counter-propagating laser. Via Compton backscattering process, the electron bunch radiates high energy X-rays or gamma-rays. The photon energy is given by $4\gamma^2\varepsilon_L$ approximately where γ is the Lorentz factor of an electron and ε_L the laser photon energy. The temporal profile of the radiation spectrum has the same shape as that of the energy distribution of the electron bunch. When the CEP-locked 5 fs full-width half-maximum (FWHM) laser has a cosine shape, which means that the strongest field is at the center of envelope, only small a part of the electron bunch has the highest energy, leading to the burst of highest energy photons only during a fraction of a laser cycle. When a spectral filtering using a crystal spectrometer is applied [14, 15, 16, 17], one is able to attain an isolated attosecond gamma-ray.

3. Simulation

To demonstrate this scheme, a series of simulations have been carried out. The electron dynamics is calculated by solving numerically a relativistic equation of motion. A paraxial Gaussian beam approximation is used to describe a focused laser field [18]. The magnetic field by the single-period wiggler is expressed as follows:

$$\vec{B} = \begin{cases} \hat{y}B_0 \sin\left(\frac{2\pi}{\lambda_w}z\right) & (-\lambda_w/2 < z < \lambda_w/2) \\ 0 & \text{elsewhere} \end{cases} \quad (1)$$

The detail of the calculation methods for the dynamics and the radiation are described in [19, 20, 21]. The interactions among the electrons are ignored because the laser field is much stronger. The Thomson-scattered radiation is calculated using formula derived by Brown and Hartman [22]. The radiated photon number N_S from an electron is described as

$$\frac{dN_S}{d\epsilon d\Omega dt} = c(1 - \vec{\beta} \cdot \hat{k}_L)n_L(\vec{r}, t) \frac{1}{\sqrt{\pi}\Delta\epsilon_e} \exp\left[-\frac{(\epsilon - \epsilon_S)^2}{\Delta\epsilon_e^2}\right] \frac{d\sigma}{d\Omega} \quad (2)$$

where c is speed of light, $\vec{\beta} = \vec{v}/c$ when \vec{v} velocity of the electron, \hat{k}_L the propagation direction unit vector of the counter-propagating laser, and n_L the photon number density on the electron position \vec{r} and time t . $d\sigma/d\Omega$ is the differential cross section for Thomson scattering and is a function of the electron velocity direction, the detector direction and the laser polarization. ϵ is the radiated photon energy and ϵ_S the central photon energy of the radiated photon energy distribution. $\Delta\epsilon_e = \Delta\epsilon/(2\sqrt{\ln 2})$ where $\Delta\epsilon$ is the FWHM spectral width of the radiation. They have a relation of $\Delta\epsilon = (2h \ln 2 / \pi \Delta t_L)(\epsilon_S/\epsilon_L)$, where h is the Plank constant and Δt_L the FWHM pulse width of the driving laser. The central photon energy ϵ_S ($\epsilon = \hbar\omega$ and $\hbar = h/2\pi$) is calculated by relativistic Doppler effect (Eq. (3), (5)) [22] and recoil (Eq. (4)) [23] as following relations:

$$\frac{\omega'_L}{c} = \frac{\omega_L}{c} \gamma (1 - \vec{\beta} \cdot \hat{k}_L) \quad (3)$$

$$\hbar\omega'_S = \frac{\hbar\omega'_L}{1 + (1 - \cos\theta'_{L-S})\hbar\omega'_L/mc^2} \quad (4)$$

$$\omega_S = \frac{\omega'_S}{\gamma(1 - \vec{\beta} \cdot \hat{k}_S)} = \frac{\omega'_S}{\gamma(1 - \beta \cos\theta_e)} \simeq \frac{2\gamma\omega'_S}{1 + \gamma^2\theta_e^2} \quad (5)$$

where ω_L and ω_S are the angular frequency of the driving laser and radiation in the lab frame, respectively, and the primed variables, ω'_L and ω'_S are for the rest frame of an electron. \hat{k}_S is the propagation unit vector of the radiation, θ'_{L-S} the angle between the driving laser and the radiation in the rest frame, θ_e the angle between the velocity of the electron and the radiation. The direction of the radiation means the opposite direction of the line of sight of a detector. The angular frequency of the driving laser in the lab frame ω_L is converted to that in the electron's rest frame ω'_L by Eq. (3). The recoil effect, the energy loss between incident ω'_L and scattered photon ω'_S is considered in Eq. (4). The scattered photon energy in the lab frame ω_S is calculated from ω'_S using the relation of Eq. (5). When the electron energy is small, the photon energy in the electron's rest frame is much smaller than electron's rest mass but for the higher energy of an electron, the recoil needs to be considered because the photon energy in the electron's rest frame becomes noticeable. For instant, when a laser of 532 nm wavelength is backscattered by an electron of 530 MeV energy, the central energy of the scattered photon is lowered by 1.9 % due to recoil effect.

In the simulation, an 800 nm, 0.25 mJ and 5 fs FWHM laser is used to modulate the electron bunch energy. The laser is CEP locked so that the peak of the envelope coincides with the peak of the field. The laser is focused to a beam waist of 100 μm at the center of the wiggler. A beam waist w_0 means the radius at which the intensity decreases to $I_0 \exp(-2)$ when I_0 is the peak intensity. The peak intensity is $2P_0/(\pi w_0^2) = 3.2 \times 10^{14} \text{ W/cm}^2$ for the peak power of the laser of $P_0 = (0.25 \text{ mJ})/(5 \text{ fs}) = 50 \text{ GW}$. The electron bunch used in the simulation has 240 MeV energy with an energy spread of 0.1 %. The length of the bunch is 30 μm with a normalized emittance of 2 mm mrad. The bunch is also focused to a beam HWHM (half width at half maximum) radius of 30 μm at the center of the wiggler. The magnetic field by the wiggler is described by Eq. (1) with B_0 of 0.5 T and λ_w of 3 cm.

4. Energy modulation of electron bunch

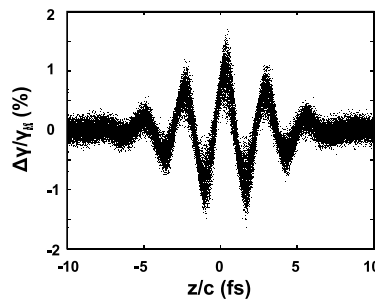


Fig. 2. Electron energy distribution after the chicane. $\Delta\gamma/\gamma_0 = (\gamma - \gamma_0)/\gamma_0 \times 100$ (%) when γ_0 is the initial average Lorentz factor

Figure 2 shows the energy distribution of the electron bunch after interacting with the laser field in the wiggler and passing chicane. The change in the relative position between each of the electrons due to the difference in the velocities is canceled by the chicane. Note that the temporal profile of the laser field is duplicated into the energy distribution of the electron bunch.

When an electron interacts with a laser field under the magnetic field by the wiggler, $d\gamma/dt$ is proportional to $-p_x E_L$, where p_x is the x -component of the relativistic momentum, $\gamma m \vec{v}$, of the electron and E_L the electric field seen by the laser on the electron and m the electron's mass. [24] Then the degree of the energy modulation is determined by the integration of $-p_x E_L$ over the interaction time or distance: $\Delta\gamma \propto -\int p_x E_L dt = -\int p_x E_L dz/v_z$, when p_x and E_L are the quantities experienced by the electron. The modulation is plotted in Fig. 3(a) with respect to the magnetic field strength, B_0 . For given specifications of the laser and electron beam under consideration, the modulation increase with B_0 , reaches the maximum of 1.1 % at $B_0 = 0.5 \text{ T}$ and then decrease eventually to 0.45 %. To understand this behavior, we need to look at both p_x and E_L in more detail. p_x and E_L are plotted in Fig. 3(b) for different B_0 . From the equation of motion, it is easily seen that p_x is proportional to the integration of the wiggler magnetic field over the interaction distance. Hence from Eq. (1), p_x is just a cosine function and is always smaller than zero. By changing B_0 , only the amplitude of p_x is changed. Now E_L , the electric field of the laser seen by the electrons, varies with respect to B_0 . This variation comes from the slippage between the electron and the laser. Even though the electron moves relativistically, it still moves slowly compared to the laser. Furthermore when the electron moves under the wiggler magnetic field, its trajectory is curved and more curved for stronger field. Figure 3(c)

shows the slippage that the electron experiences for different strengths of the magnetic field. The slippage is less than a quarter cycle for $B_0 = 0.5$ T [solid line] and about 1.5 cycle for $B_0 = 1.2$ T [dotted line]. The corresponding electric fields are shown in Fig. 3(b). When becomes larger than 0.5 T, the sign of the electric field changes, making a negative contribution to the energy modulation ($\Delta\gamma \propto -\int p_x E_L dt$). This leads to the maximum modulation taking place at $B_0 = 0.5$ T. There is a local minimum at 1.0T because the electron sees one cycle of the laser and the modulation accumulated by the first half cycle is now eaten up in the second half cycle. At 1.2 T, the electron experiences one and half cycles of the laser field and the 3rd half-cycle increases the modulation, resulting in the 2nd maximum.

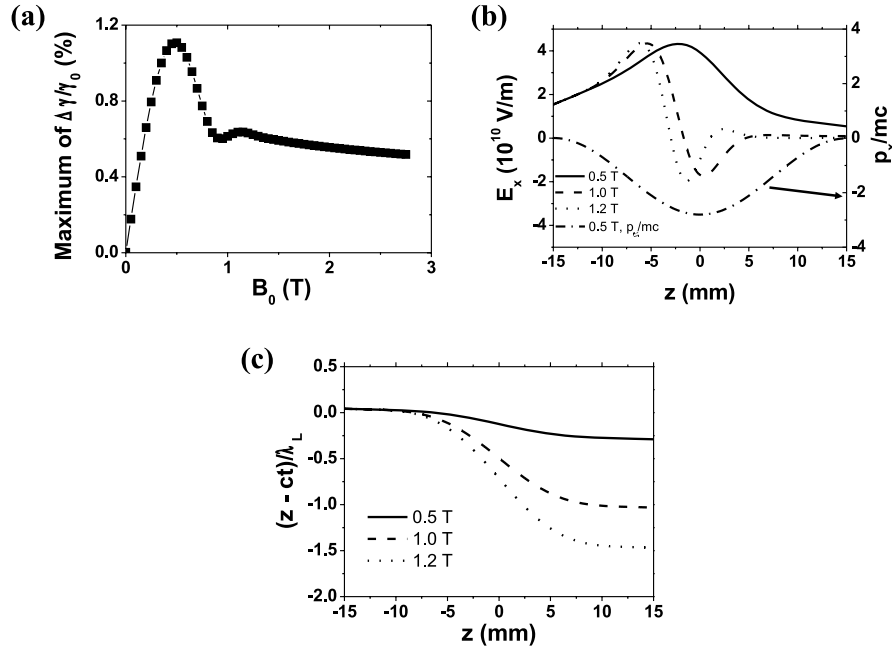


Fig. 3. (a) The maximum value of the $\Delta\gamma/\gamma_0$ for each of the peak magnetic field B_0 . Each value calculated for a line shape bunch with no emittance. (b) The laser electric field seen by the electrons for each peak magnetic field and $p_x/(mc)$ for $B_0 = 0.5$ T. The shape of the $p_x/(mc)$ is the same for different B_0 and its amplitude is just proportional to B_0 . (c) The slippage of the electrons from the laser field. λ_L is the laser wavelength.

5. Attosecond gamma-ray pulse

The energy-modulated electron bunch interacts with a counter-propagating laser, radiating gamma-rays via the Compton backscattering. The temporal profile of the spectrum is also modulated as shown schematically in Fig. 4(a). The spectral filtering with a crystal spectrometer to pick the photons of the highest energy may lead to the attainment of an attosecond pulse as shown in Fig.1. There are three major points to consider for the attainment of an isolated attosecond pulse: (1) the modulation depth [A in Fig. 4(a)] should be as large as possible for higher photon flux and better contrast ratio, (2) the spectral width [B in Fig. 4(a)] at a given time is narrow and (3) the temporal width [C in Fig.4(a)] should be small. Four points contribute to the spectral width: the energy spread of the electron bunch (~ 0.1 %), the bandwidth of a driving laser, Doppler effect and recoil effect. The bandwidth ($\Delta\epsilon$) of the radiation due to

the bandwidth ($\Delta\varepsilon_L$) of the driving laser has a relation of $\Delta\varepsilon/\varepsilon_S \simeq \Delta\varepsilon_L/\varepsilon_L$. For the driving laser of a 100 fs FWHM, 532 nm light, $\Delta\varepsilon/\varepsilon_S \simeq 0.78\%$. For the attainment of an isolated attosecond pulse, the modulation depth should be at least larger than 0.78%; otherwise, there will be a small prepulse one cycle earlier than the main pulse. For a 10 ps FWHM, 532 nm laser light, $\Delta\varepsilon/\varepsilon_S \simeq 0.0078\%$. The requirement for the modulation depth is much less stringent. Another effect of the large bandwidth is that in view of spectral filtering, the larger bandwidth (large B) leads to a longer pulse width of the radiation from an electron bunch. The temporal width (C) is the pulse duration of the radiation from a single electron interacting with the counter-propagating driving laser, given by $\Delta t = \Delta t_L/4\gamma^2$ where Δt is the pulse width of the radiation from a single electron. For a 10 ps FWHM pulse, the radiation duration (C) by a single electron of 240 MeV is 11.3 as; on the other hand, 1.13 fs for a 1 ns FWHM laser pulse. For the generation of attosecond pulses, the pulse duration of a driving laser should be much shorter than 1 ns FWHM.

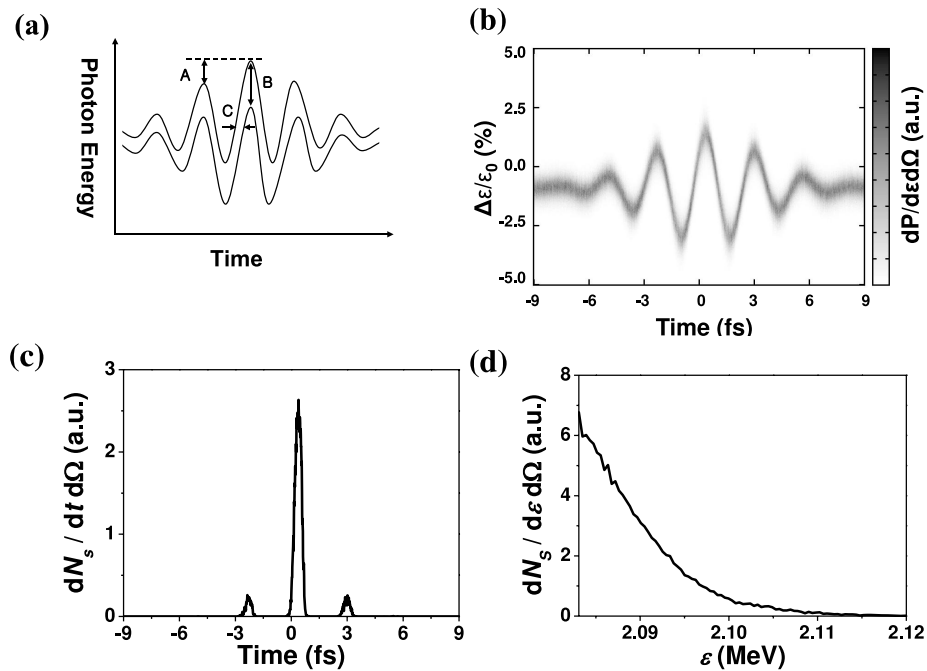


Fig. 4. (a) Schematic diagram for the temporal distribution of the radiation spectrum from Compton backscattering of the energy modulated electron bunch with the laser. (A: modulation depth, B: spectral width, C: temporal width) (b) The spectral and temporal distribution of the radiation. $\Delta\varepsilon/\varepsilon_0 = (\varepsilon - \varepsilon_0)/\varepsilon_0 \times 100(\%)$ when ε is the photon energy and $\varepsilon_0 = 4\gamma^2\varepsilon_L = 2056$ keV. (c) Temporal profile of radiation power above $\Delta\varepsilon/\varepsilon_0 > 1.3\%$ which shows a 430 as gamma-ray pulses at 2.1 MeV (d) The spectrum of (c).

The spectral width is also increased due to the relativistic Doppler effect and the recoil. As shown in Eqs.(4) and (5), the angular frequency ω_S is a function of the interaction angle between the laser and electron. It means that the photon energy changes with respect to the detecting angle. The proper selection of a particular spectral region for isolated attosecond pulse, the angular width by a detector has to be limited. The calculations shows that the spectral broadening due to Doppler effect and recoil effect is 0.25% and 0.0091% for the detection angular width of $0.05/\gamma$ on axis and an electron energy of 530 MeV, respectively. The spectral

broadening due to recoil effect is negligible in our study.

Considering these points, a 532 nm, 100 mJ and 10 ps FWHM laser is chosen as a driving laser. The 1 nC, 100 fs, 240 MeV electron bunch (energy-modulated) is focused to a beam radius of 30 μm and the laser to a beam waist of 30 μm at the interaction point for Compton backscattering. Figure 4(b) shows the temporal and spectral distribution of the radiation from the modulated electron beam. The radiation is detected from the angular region of $\theta_D \leq 0.03/\gamma$ when θ_D is polar angle from the z-axis.

If we cut off at the level of 1.3 % modulation and take higher energy photons from the total radiation [Figure 4(b)], it is expected to obtain a 430 as FWHM pulse with a contrast ratio against the background of about 10.2:1 [Figures 4(c)]. Figure 4(d) shows the spectrum of the gamma-ray pulse. For a 1 nC electron charge, 7.0×10^1 gamma-ray photons are expected to be produced as 430 as pulse. If smaller contrast ratio and longer pulse width is allowed the photon number can be increased. When the angular region becomes wider to $\theta_D \leq 0.05/\gamma$ and the cut-off modulation level becomes lower to 1.2 % the photon number grows to 2.2×10^2 , pulse width increases to 490 as and the contrast ratio becomes worse to 5.1:1. As explained in the previous paragraph, the pulse width will be increased to 540 as for a counter-propagating laser of 500 ps pulse width. When the laser pulse width is decreased to 200 fs, the contrast ratio becomes worse to 4.4:1.

One may claim that the photon number per pulse of 2.2×10^2 is too small for application. The photon number is small just because the radiation duration is quite short. The photon number/second can be increased by increasing the laser energy or the repetition rate. Currently, a laser of 1 J at 100 Hz is available. Using this laser, the photon number is increased by a factor of 1000. Since the laser technology advances very fast, a higher flux of gamma rays from Compton source is expected. [25]

The tunability of the photon energy of the radiation is also tested. When a 60 MeV electron bunch, a 1064 nm driving laser and a wiggler of 0.07 T is applied, a 550 as, 64 keV X-ray pulse with a photon flux of 2.1×10^2 is generated. For the higher energy gamma-ray, the electron bunch of 530 MeV energy, a wiggler of 1.1 T and a 532 nm laser can be used to produce a 380 as, 10 MeV gamma-ray pulse with a flux of 3.2×10^2 . The details of the conditions and results are listed in Table 1.

To demonstrate the result of this simulation in real experiments, a spectral filter is required. One candidate for this purpose is a crystal spectrometer. Two types of spectrometer using a crystal as grating have been popular in gamma-ray region: a curved crystal spectrometer [15, 16] and a double-flat-crystal spectrometer. [17] The curved crystal spectrometer is adopting a curved quartz crystal and has advantage of higher efficiency than the double-flat-crystal spectrometer. It can measure the gamma-ray photon energy up to 1.5 MeV with a resolution being higher than 0.1 % for the reflection order higher than 2. The resolution of 0.1 % is enough to cut off the photons of the lower energy in this scheme. The double-flat-crystal spectrometer, equipped with two flat Si or Ge crystals, has lower throughput and higher resolution than curved crystal spectrometer. It can be used in the photon energy range up to 6 MeV. There are no proper solution in the range over 6 MeV. The generation of an attosecond gamma-ray pulse of the photon energy of 10 MeV seems difficult with current technology.

Because the modulation is determined by the laser, the time jitter is in the order of 100 as and it is well suitable to the pump-probe experiments. Generally, electron based photon sources have about 1 ps time jitter because of the jitter of the electron gun. [26]

6. Summary

In conclusion, a new method to generate an isolated attosecond gamma-ray is proposed. When an electron bunch co-propagates with a few-cycle CEP locked laser, the laser field pattern is

Table 1. Simulation conditions and results mentioned in this paper. Each column lists one set of conditions and the result from it. The data of second column, which has the electron energy of 240 MeV and the detecting angular range of $\theta_D \leq 0.03/\gamma$, is about the Fig 4(b), (c) and (d). It is optimized aiming at the contrast of 10 and other data at the contrast of 5.

Energy modulation of electron bunch				
Electron energy	60 MeV	240 MeV		530 MeV
Normalized emittance	2 mm mrad			
Electron bunch radius	30 μm			
Laser wavelength	800 nm			
Laser pulse width	5fs			
Laser energy	0.25 mJ			
Laser beam waist	30 μm			
Wiggler period	3 cm			
Wiggler peak magnetic field	0.07 T	0.5 T		1.1 T
Compton backscattering and spectral selection				
Laser wavelength	1064 nm	532 nm		
Laser pulse width	10 ps			
Laser energy	100 mJ			
Electron bunch charge	1 nC / 100 fs			
Electron bunch radius	30 μm			15 μm
Laser beam waist	30 μm			20 μm
Detecting angle	$\theta_D < 0.05/\gamma$	$\theta_D < 0.03/\gamma$	$\theta_D < 0.05/\gamma$	$\theta_D < 0.04/\gamma$
Cutoff energy ($\Delta\epsilon/\epsilon_0$)	2.2 %	1.3 %	1.2 %	1.5 %
Radiated pulse				
Photon energy	64 keV	2.1 MeV		10 MeV
Contrast ratio	5.1:1	10.2:1	5.1:1	5.4:1
Pulse width	550 as	430 as	490 as	380 as
Photon number per shot	2.1×10^2	7.0×10^1	2.2×10^2	3.2×10^2

copied to the energy distribution of the electron bunch. By Compton backscattering, the electron energy distribution is duplicated to the temporal photon energy distribution of the radiation. When the highest photon energy is chosen, only a small part of the radiation is temporally selected. After cutting off the lower energy photons, an isolated attosecond pulse is left. In the simulation, a 5 fs FWHM laser and a 3-cm long single-period wiggler are used to modulate the energy of an electron bunch of a 240 MeV. The generation of an isolated 490 as gamma-ray pulse is demonstrated for a driving laser of a 532 nm, 10 ps FWHM. When the charge of the electron bunch is 1 nC and the laser energy is 100 mJ, the photon number of the gamma-ray pulse is 2.2×10^2 at an photon energy of 2.1 MeV. The photon energy of the attosecond pulse is tunable from 64 keV to 10 MeV or higher energy. The tunable, well-polarized, attosecond gamma-ray will certainly add a new dimension to the exploration of nature.

Acknowledgment

We acknowledge useful discussions with F. V. Hartemann and F. Krausz. This work has been supported in part by BK21 project funded by the Korea Research Foundation and in part by Basic Research Program (Grant No. KRF-2008-313-C00356) funded by Korean Research